7th World Congress on Structural and Multidisciplinary Optimisation
COEX Seoul, 21 May – 25 May 2007, Korea

Smooth Boundary Based Optimisation Using Fixed Grid

Caroline S Edwards[1], **H Alicia Kim**[1], **Chris J Budd**[2]

[1]Department of Mechanical Engineering, University of Bath, United Kingdom. C.S.Edwards@bath.ac.uk
[2]Department of Mathematical Sciences, University of Bath, United Kingdom.

1. Abstract

This paper presents a boundary based structural optimisation in the finite element fixed grid environment. The boundary is represented by smooth B-spline curves, as they typically require a relatively small number of control points to describe a curve. Utilising B-spline control points reduces the number of design variables whilst achieving a smooth boundary representation. An appropriate control point coordinate modification formulation with addition/removal of control points, derived from the optimality criteria of compliance based optimisation, is introduced in the paper. The paper also examines a range of structural analysis solvers appropriate for frequent boundary modifications in topology optimisation. Previous studies have found that iterative pre-conditioned conjugate gradient solvers with appropriate pre-conditioners were most efficient for analysis and reanalysis. Whilst it has been shown that LU decomposition of the stiffness matrix can offer a fast convergence for reanalysis, it cannot guarantee convergence. The performance of the pre-conditioned conjugate gradient solver for optimisation is carefully studied with some of the latest direct solvers developed for elasticity and FE problems. The careful implementation of the analysis solver together with the reduced number of design variables achieves an efficient and structural optimisation scheme. This is demonstrated in the paper numerically via simple shape optimisation problems, followed by preliminary results for topology optimisation.

2. Keywords: Fixed grid, Boundary optimisation, Topology optimisation, B-splines

3. Introduction

In a fast and continually growing world where computational power is ever increasing, the need for efficiency continues to be prevalent. Structural topology optimisation is a research field which is heavily reliant on computational power. Structural topology optimisation also has a reliability requirement, which currently is heavily reliant on numerical parameters whose appropriate values can sometimes be transparent [1, 2].

Reliability issues surrounding the results of topology optimisation are largely due to the coupling of the optimisation method with the finite element (FE) mesh. One such occurrence is the inability of a method to produce a discrete solution. Solid isotropic microstructure with penalisation (SIMP) [3], [4], [5] is a topology optimisation method which uses the continuous material distribution of the problem as the design variable. Problems with continuous design variables tend to result in optimal designs which are also continuous. Thus to encourage a discrete design, penalties are applied to the continuous design variables. However, this introduction of penalisation can introduce multiple local optima [6], [2].

Another reliability issue with topology optimisation methods is the dependency on the shape of the finite elements. A simple and thus popular element choice is 4-node quadrilateral elements which take the shape of a square. The square shape of the element can give rise to re-entrant corners, which in turn causes numerical instabilities. Evolutionary structural optimisation (ESO) is one method which in particular suffers from problems with re-entrant corners [7], [2]. Also, the combination of piecewise linear elements and piecewise constant material design variables can result in numerical instabilities [8]. These numerical instabilities can produce an undesirable formation of chequerboard patterns of solid and void material within the optimal topology [9]. Various methods have been suggested to overcome numerical instabilities; such as the use of filtering techniques to smooth out local sensitivity concentrations [10].

Recently a number of topology optimisation methods were introduced which attempt to decouple optimisation from the FE formulation. One such method combines a concept known as fixed grid (FG) [11] for the finite element analysis with the topology optimisation method ESO [12]. FG is a mesh free FE method where the structural boundaries are superimposed onto an FE mesh. As in previous topology optimisation methods, the stiffness of elements that are inside or outside of the boundary is altered to reflect the solid or void nature of the element. The stiffness of the elements on the boundary is also altered to reflect the bi-material nature of the element.

The implementation of FG with ESO predominantly uses boundary points joined linearly, in which one boundary point is defined per element, to model a boundary for a structure [12]. Therefore, the resulting topology is not as smooth as it can be and a vast number of design variables is used to modify the boundary.

The extended finite element method (XFEM) [13] is also a method which can model holes within a structure without the need to rebuild the mesh. Originally designed to model crack growth, XFEM enriches the FE approximation using additional functions. The additional functions model the cracks and holes within the structure.

Another method which decouples optimisation from the FE mesh is the use of level sets [14] in conjunction with shape optimisation to model the boundaries of a structure [15], [16]. The level set formulation produces smooth boundaries; however, changing the topology of structure is not a straight forward task and is thus an active field of research. One emerging idea is the use of topological derivatives [17] to calculate potential hole locations and combining them with the level set optimisation [18], [19], [20].

The aim of this paper is to develop an efficient and reliable topology optimisation by using FG. In addition to the efficiency of FG in reanalysis, a range of direct solvers are investigated to determine the most suitable solver for optimisation with fast solution time and reliable convergence. The efficiency of optimisation is also addressed by implementing B-spline control points as design variables thereby reducing the number of design variables.

The outline of this paper is as follows: the next section details the FG approximation. Section 5 contains details of the test problems which are used within this paper both for the linear solver investigation and for application of the optimisation method. The linear solver investigation is performed also in section 5. The problem formulation and optimisation algorithm is outlined in section 6. Section 7 contains the application of the boundary based optimisation method to the previously defined test problems. Section 8 outlines the modifications made to the shape optimisation algorithm to incorporate topology optimisation along with the preliminary results, which is followed by conclusions.

4. Fixed Grid Approximation

In the FE environment, a set of n elements over a design domain Ω is used to represent a structure. Fixed grid is used within this FE environment to quickly solve linear elasticity problems such as (1), for global stiffness matrix $\mathbf{K}$, load vector $\mathbf{f}$ and displacement vector $\mathbf{u}$.

$$\mathbf{Ku} = \mathbf{f} \tag{1}$$

Fixed grid is different from the traditional FE approach in that a structure is represented by a rectangular area of regular sized elements rather than the fitted mesh, as shown in Figure 1. Each element within the domain is assigned material properties which reflect the status of the element. There are three types of element which are also shown in Figure 1: the first is the inside element (I), where all 4 nodes of an element are contained within the boundaries of the structure; the second type of element is the outside element (O), where all 4 nodes of the element are outside the structures boundaries; the third element type is on the boundary and is partially inside (B).

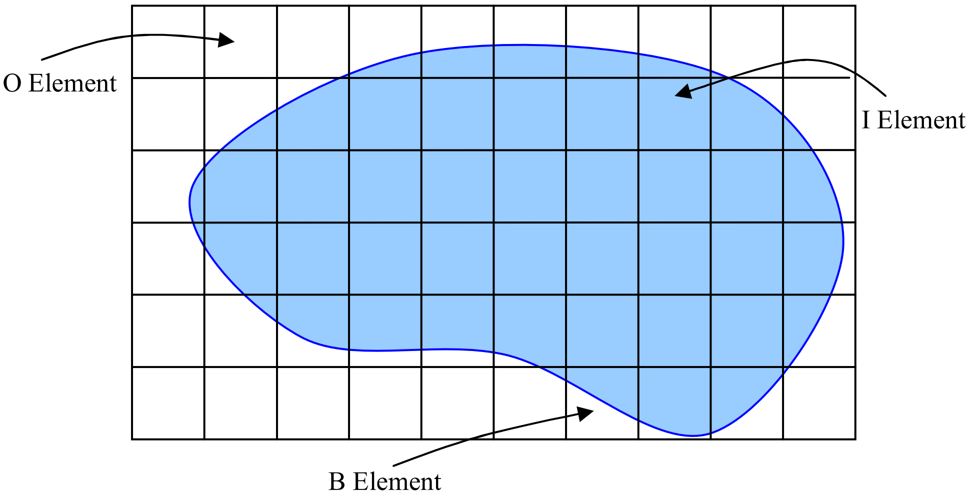

Figure 1: Fixed grid domain with superimposed topology in grey, showing inside (I), outside (O) and Boundary (B) elements

The boundary elements are modelled as a linear homogenisation of inside and outside elements based on their respective area ratios. Whilst the model will reduce the accuracy of the FE approximation, the modelling is simple to implement and the stiffness matrix $\mathbf{K}$ is easy to update without the need to completely regenerate. Also, since the FG elements can have partially inside elements, the design variable of elemental density is no longer piecewise linear, thus avoiding the numerical instabilities such as the chequerboard phenomenon, where the optimum topology contains a chequerboard pattern of solid and void material. Thus FG is ideally suited for structural optimisation [11].

The continuous variable x is used to represent the linear area ratio of material. For an element e, the element stiffness $\mathbf{K}_e$ can be written in terms of $\mathbf{x} = \{x_1, x_2, \ldots, x_n\}$ as

$$\mathbf{K}_e = x_e \mathbf{K}_0, \tag{2}$$

where $x_e \in (\delta,1]$, δ is a value that is close to 0, and $\mathbf{K}_0$ is the element stiffness constant with $x_e = 1$. For an inside (I) element, x_e takes the value '1' and for outside (O) elements, x_e takes the value 'δ' to maintain a non-singular stiffness matrix. Boundary (B) elements have $x_e = a_B$ where a_B is the area ratio of the B element.

5. Investigation of Linear Solvers

The regularity of FG offers a unique opportunity for the exploitation of a consistent structure of the stiffness matrix. A fixed grid with sequentially ordered elements will provide a consistent connectivity between structural degrees of freedom. Since the fixed grid is independent from the geometry of a structure, the stiffness matrix **K** will have a virtually constant structure. Thus the efficiency of a number of linear solvers is investigated using the design domains of a short cantileverd beam of aspect ratio 1.6 and the popular 'Michell' type structure [21] shown in Figure 2.

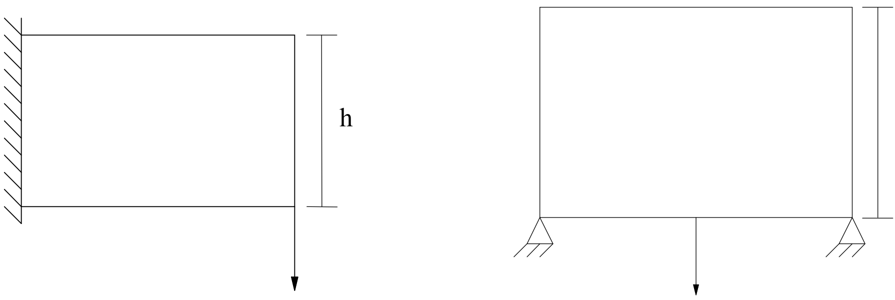

(a) Short cantilever (b) 'Michell' type structure

Figure 2: Test problems

5.1. Stiffness matrix structures of test problems

The connectivity of the stiffness matrix in FG is only dependent on the number of elements and the structure of the stiffness matrices associated with the test problems can be identified, Figure 4.

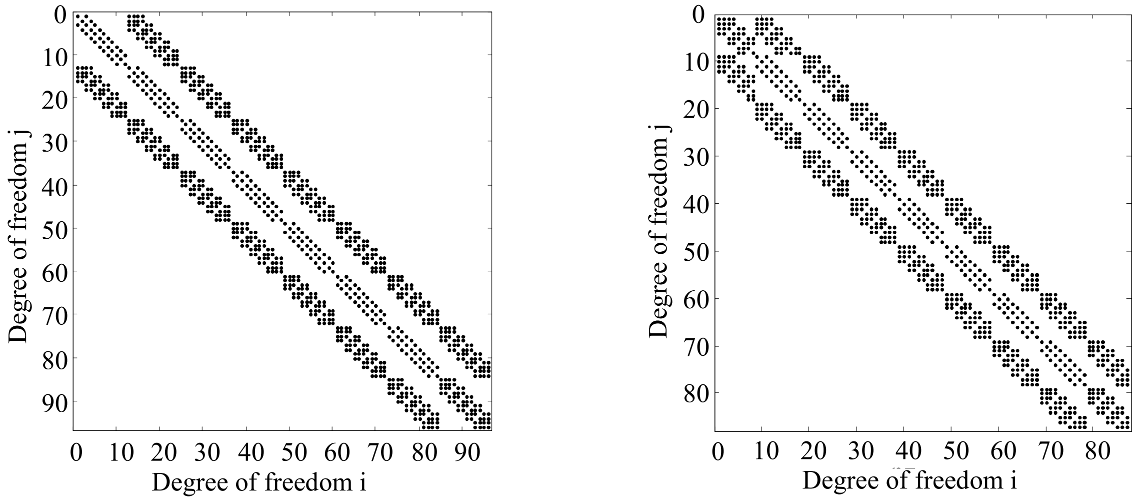

(a) Short cantilever beam (b) 'Michell' type structure

Figure 3: Graphical representation of the structure of the FG stiffness matrix. The black dots represent non-zero entries

From Figure 3, it is clear that FG stiffness matrices are of a similar structure. Both matrices are tri-diagonally banded matrices which are vastly sparse, but the similarities are much more than that. The maximum band size of each diagonal is the same, the pattern created the outer diagonal entries take the same pattern and the central diagonal entries generally take the same pattern with any differences caused through the boundary conditions. Thus the linear solvers to be investigated are those suitable for sparse, banded, positive definite matrices.

5.2. Frontal Solvers

Frontal solvers are direct solvers which have their origins in the solution of FE problems [22], however, they can also be applied to fully assembled matrices. They use the connectivity information of the finite elements to efficiently implement Gaussian elimination. The Gaussian operation is performed once all of the terms for a degree of freedom have been entered and the matrix has been permuted so that the entry is in the next pivotal position. Therefore the Gaussian elimination and the assembly of **K** can be interleaved and so the matrix is never assembled explicitly. The degrees of freedom that have entries in the stiffness matrix **K** but have not yet been eliminated are referred to as active elements and form a front in the symmetrically permuted stiffness matrix; hence the technique is called the frontal method.

5.3. Multifrontal solver

Whilst the frontal solver is assembled by adding one element stiffness matrix $\mathbf{K}_e$ to the global stiffness matrix **K** at a time, the multifrontal method assembles element stiffness matrices in pairs. Then the bi-element stiffness matrices are assembled in pairs and so forth. This method then has multiple fronts, hence the name and keeps the size of the fronts to a minimum. Less computation is required to assemble matrices with smaller fronts, thus producing a more efficient linear solver.

5.4. Band Solver

Finally, a solving method which exploits the banded nature of FG stiffness matrices is considered. When the finite elements are numbered in an efficient manner, the resulting stiffness matrix can be banded with a relatively small band. Fixing particular degrees of freedom for a specific structure such as the short cantilever or the Michell structure detailed above can reduce the band for a particular row within the stiffness matrix. When the maximum band size along with the band size for each row is known *a priori*, as it can be for the stiffness matrix, the matrix structure can be exploited when attempting to solve.

A popular method for solving linear systems with non-zeros pivots is to decompose the matrix, such as the stiffness matrix, into a lower triangular matrix **L** and an upper triangular matrix **U**. This method is referred to LU decomposition. However, when the matrix is symmetric and positive definite, like a stiffness matrix **K**, the factors of **U**, can be chosen such that they are those of the transpose of **L**. This special case of matrix decomposition is referred to as Cholesky factorisation and is twice as efficient as LU decomposition as only half of the number of entries is required. Cholesky factorisation is a suitable factorisation method for banded matrices, even when the actual band width varies as it does with the stiffness matrix, since the lower triangular matrix **L** will have the banded structure of the matrix to be decomposed and the only entries that are required to be calculated are those within the row band.

HSL libraries (MA62, MA57 and MA55) using an Intel® Fortran complier were used for this investigation [23].

5.5. Application of Linear Solvers to Test Problems

The mesh density of both the short cantilever and the 'Michell' type structure is varied considerably in the first instance. The average CPU times taken to solve the linear system (1) in each case are recorded and are presented in Figure 4.

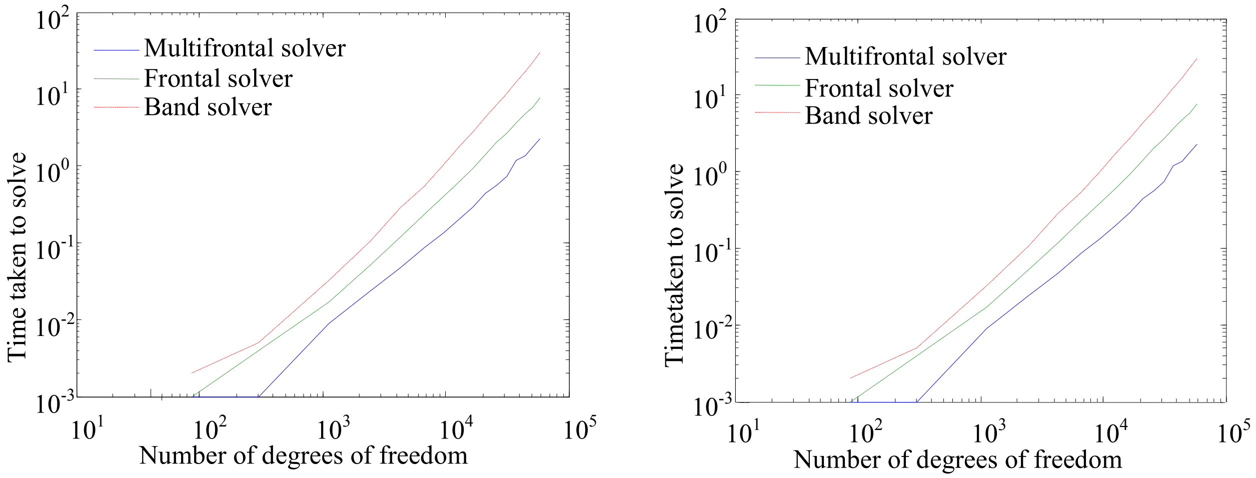

(a) Short cantilever

(b) 'Michell' type structure

Figure 4: Variation of solution time for varying numbers of degrees of freedom

It is clear from Figure 4 that the frontal solvers are much more efficient solvers for this FE problem than for the band solver. The band solver uses a lot of memory as the entire band is required. Figure 3 shows that there are a number of non-zero entries inside the band which all require storing and factorising. The frontal solvers only require the non-zero entires to be stored. All three methods have efficient factorisation techniques, however the band solver requires significantly more memory which slows the solution time down considerably.

The frontal solvers have considerably less solution time than the band solver. However, in both cases the use of multiple fronts in a general solver has proved to be far more efficient than using a single front is a specifically designed solver. It is therefore clear that the use of multiple fronts has significant computational savings for large sparse linear systems.

5.6. Direct vs Itrative Linear Solver

Iterative solvers such as a pre-conditioned conjugate gradient solver [25] use significantly less memory to solve since the process is iterative. So for large problems where there are around 10^6 degrees of freedom, the memory savings produce a more efficient solver. Therefore, pre-conditioned conjugate gradient solvers are widely used with FE problems, (see for example [11], [24]).

Fixed grid has been implemented using a pre-conditioned conjugate gradient solver which exploits the symmetrical positive definite structure and uses Jacobi pre-conditioning [11]. The multifrontal linear solver is compared to this conjugate gradient solver with a Jacobi pre-conditioner using a modest number of degrees of freedom.

Figure 5 clearly shows that the multifrontal solver is a significantly faster linear solver than the conjugate gradient solver with Jacobi pre-conditioner. There are 3 main reasons why the multifrontal solver is faster in this instance compared to the pre-conditioned conjugate gradient solver. The first reason is the modest number of degrees of freedom considered. The significant savings made by pre-conditioned conjugate gradient solvers are not apparent at this level. The memory savings become more apparent with larger problems. However, the multifrontal solver on an Intel® Pentium 4 3.0 Ghz machine with 1G RAM, when complied using the Intel® fortran complier, can solve a system with 10^6 degrees of freedom in under 200s.

The multifrontal solver is advantaged over the pre-conditioned conjugarte gradient solver used in this investigation as the multifrontal solver is programmed using Fortran 77 whereas the CG solver uses C++, which can be less efficient for numerical computations. .is faster is due to the multifrontal solver is much faster is due to Direct solvers also have added an advantage that the convergence is always guaranteed. Thus the multifrontal solver is implemented as the linear solver for the FG finite element analysis.

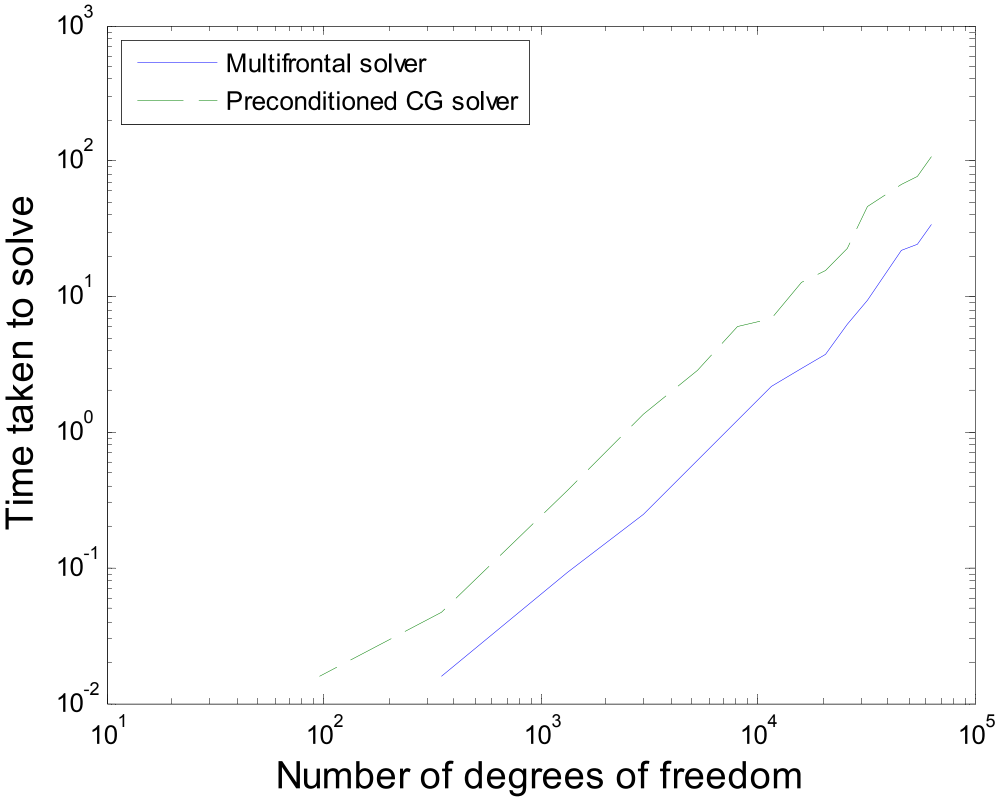

Figure 5: Variation of solution time for varying numbers of degrees of freedom

6. Formulation for structural Optimisation

In this section, the formulation for the optimisation is presented, along with a sensitivity analysis and the optimisation algorithm.

6.1. Objective Function
The objective function is defined to minimise the compliance volume product. Letting the thickness of an element *f* be v_f and the compliance-volume product be $S(\mathbf{x})$ as represented in (3), the optimisation problem can be written as

$$\left.\begin{aligned} &\min_x : S(\mathbf{x}) = CV = \mathbf{u}^T\mathbf{K}\mathbf{u}V = \sum_e x_e \mathbf{u}_e^T \mathbf{K}_0 \mathbf{u}_e \sum_f x_f v_f \\ &: x_e \in (0,1],\ \mathrm{e} = 1,2,\ldots,\mathrm{n}. \end{aligned}\right\}. \quad (3)$$

6.2. Sensitivity Analysis
The Lagrangian *L* of the optimisation problem (3) is written as

$$L = CV + \sum_{e=1}^{n} \lambda_e^1(\delta - x_e) + \sum_{e=1}^{n} \lambda_e^2(x_e - 1), \quad (4)$$

for δ is a close to 0 as detailed above. The Lagrangian multipliers for the lower and upper side constraints are λ_e^1 and λ_e^2. An optimal solution is achieved when the derivatives of the Lagrangian function are equal to zero with respect to the design variables, that is

$$\begin{aligned} \frac{\partial L}{\partial x_e} &= 0, \text{ for } e = 1,2,\ldots,n. \\ &= \frac{\partial CV}{\partial x_e} - \lambda_e^1 + \lambda_e^2. \end{aligned} \quad (5)$$

The derivative of the Lagrangian function, for elements with constant unit thickness $v_e = 1$, is,

$$\frac{\partial L}{\partial x_e} = \mathbf{u}^T\mathbf{K}\mathbf{u} - V\mathbf{u}_e^T\mathbf{K}_0\mathbf{u}_e - \lambda_e^1 + \lambda_e^2. \quad (6)$$

Thus, for B elements, where the side constraints are inactive, the optimality condition is:

$$S_e = \frac{V\mathbf{u}_e^T\mathbf{K}_e\mathbf{u}_e}{\mathbf{u}^T\mathbf{K}\mathbf{u}} = 1. \quad (7)$$

For I elements, where the upper side constrain λ_e^2 is active and hence $\lambda_e^2 > 0$, the optimality condition is:

$$S_e = \frac{V\mathbf{u}_e^T\mathbf{K}_e\mathbf{u}_e}{\mathbf{u}^T\mathbf{K}\mathbf{u}} > 1. \quad (8)$$

Finally, for O elements, where the lower side constraint λ_e^1 is active $\lambda_e^1 > 0$, the optimality condition is:

$$S_e = \frac{V\mathbf{u}_e^T\mathbf{K}_e\mathbf{u}_e}{\mathbf{u}^T\mathbf{K}\mathbf{u}} < 1. \quad (9)$$

6.3. Optimisation Algorithm
The boundary based FG optimisation algorithm presented here removes material by slowly moving the boundaries of a structure, based on the optimality conditions (7)-(9). The slow movement of the boundaries is governed by applying move limits. An outline of the optimisation algorithm for the existing boundaries are summarised as follows:

1. The user defines 4 point locations which describe the four corners and hence the minimum and maximum

boundaries of the fixed grid

2. The user defines each set of kinematic conditions for each degree of freedom separately. A set of conditions may consist of a point condition or a series of conditions. In the case of the short cantilever of Figure 2(b), the applied load is a point condition and the clamped side is a series of conditions.
3. A spline is defined between any two sets of kinematic conditions using the point locations defined in (1). If the user wishes to preserve the symmetry of the strutcure, then extra splines can be defined to do so.
4. Control points **c** for the b-spline generation are created at equal distances along each spline. The distance between each control point is user defined.
5. Create fixed grid
6. Generate the stiffness matrix **K** and solve to find the element sensitivities S_e
7. Each spline is moved in turn by moving the control points. The movement of the control points is defined in terms of a direction and the magnitude with which it moves and is detailed below. The algorithm for the movement of the splines is limited to the removal of material from the structure, however, it can be generalised to both remove and add material.
    a. The direction of the control point movement is determined by the position of the spline close to the control point and that positions closest point to $S_e = d_i$. d_i for iteration i, is a small proportion of the optimal sensitivity $S_e = 1$ and therefore acts as a control parameter which limits the direction of movement
    b. To avoid numerical complications, the magnitude of the control point movement is limited by move limits $\mathbf{m}_i = [m_{min}, m_{max}]$ for iteration i defined in (10), where $\boldsymbol{\eta} = [\eta_{min}, \eta_{max}]$ and is user defined.

$$\mathbf{m}_i = \sqrt{1 - S_e} \cdot \boldsymbol{\eta}. \tag{10}$$

8. Determine the new distance between control points.

If the distance between two consecutive control points c_{dist} satisfies

    a. for the user defined parameter ξ_{min}, the control points are merged by removing both control points and inserting a new control point midway between the removed control points as shown in Figure 6. However, spline end control points must never be removed and in this circumstance, the two previous control points to the end control point are merged as previously described.

$$c_{dist} < \xi_{\min} \tag{11}$$

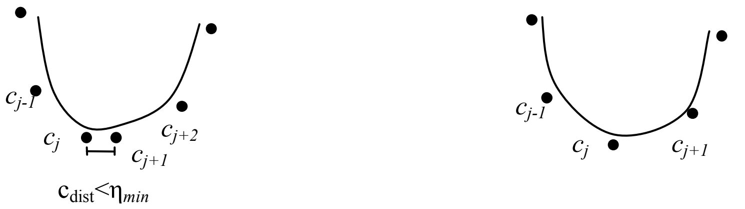

(a) Before two control points to be merged, c_j and c_{j+1} (b) New merged control point c_j

Figure 6: An example of merging 2 control points

    b. If the distance between two control points satisfies (12) for user defined ξ_{max}, a new control point is inserted midway between the two control points as shown in Figure 7

$$c_{dist} < \xi_{\max} \tag{12}$$

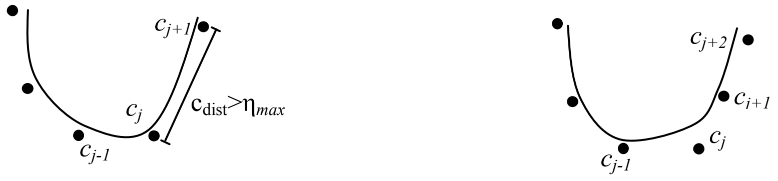

(a) Before a control point has been inserted (b) After a control point has been inserted

Figure 7: An example of inserting a control point

9. Check for oscillating solutions or solution convergence
   a. An oscillation is detected for small ε at iteration *i* if

$$\| \mathbf{c}_i - \mathbf{c}_{i-1} \| - \| \mathbf{c}_{i-1} - \mathbf{c}_{i-2} \| < \varepsilon \tag{13}$$

   b. Convergence is detected for small ε at iteration *i* if

$$\| \mathbf{c}_i - \mathbf{c}_{i-1} \| < \varepsilon \tag{14}$$

10. If neither (13) nor (14) are satisfied return to step 6, else
    a. If $d_i < 1$, increase d_i by a small amount to a maximum of $S_e = 1$and return to 7
    b. If $d_i = 1$ or the stiffness matrix becomes ill-conditioned, stop
11. Examine the modification history and select the design that is a local minimum of (3) and/or desirable volume ratio. The local and global minimum of the iteration history for a single run is henceforth referred to as the S-history local and S-history single-run-global minimum respectively.

7. Numerical Examples

In this section, the boundary based B-Spline FG optimisation algorithm described in section 6.3 is applied to the test problems of section 5.

7.1. 'Michell' Type Structures

The optimal structure for the 'Michell' type structure of Figure 2 with an (80x40) grid is obtained after 105 iterations, has a volume reduction of 49% and is presented in Figure 8(a). A plot of the minimising objective function $S(\mathbf{x})$, against iteration number is given in Figure 5(b).

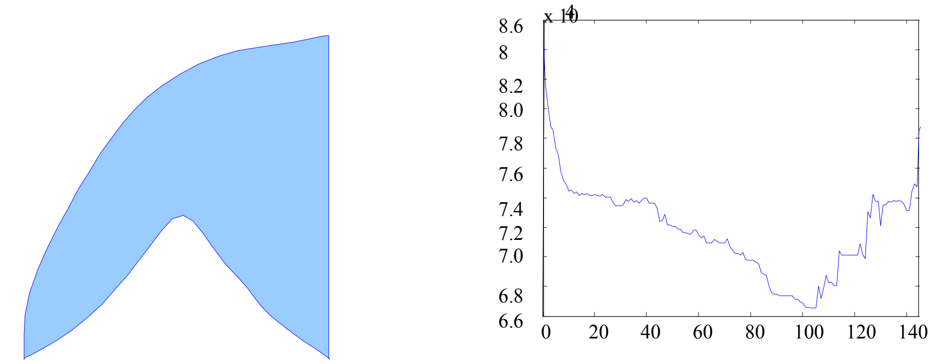

(a) Optimal Michell structure

(b) S-history of CV

Figure 8: Shape optimisation results of Michell structure

The optimisation algorithm is minimises the compliance-volume product $S(\mathbf{x})$ until iteration 105. Figure 8 shows there are some oscillations before an increase in deletion criteria. Also, an increase in deletion criteria can cause a small sudden increase in $S(\mathbf{x})$ since forcing a removal of material from a converged solution can temporarily produce a solution less optimal as it finds a new path to the a solution with less volume.

After 105 iterations, no further improvement can be made without changing the topology. Changing the topology would encourage higher sensitivity values for inside finite elements as required by (8). However, the algorithm continues to remove material and so $S(\mathbf{x})$ begins to increase as the movements produce topologies which have a less efficient use of material

7.2. Short Cantilever

The optimisation algorithm is now applied to the short cantilever test problem as described in section 5 and presented in Figure 2(b). The control point direction parameter is initially set as $d_i = 0.1$and increased by increments of 0.01. The move limits for the minimum and maximum stepsize the contol points moves are set as **mi** = (?,?) and the control points distance limits are η_{max} = ? and η_{min} = ?. A local S history minimum boundary is presented in Figure 9(a) and the variation of the objective function $S(\mathbf{x})$ is shown in Figure 9(b). The local S history minimum presented in Figure 9(a) relates to 'a' in Figure 9(b), which occurs after 115 iterations and has a 32% volume reduction.

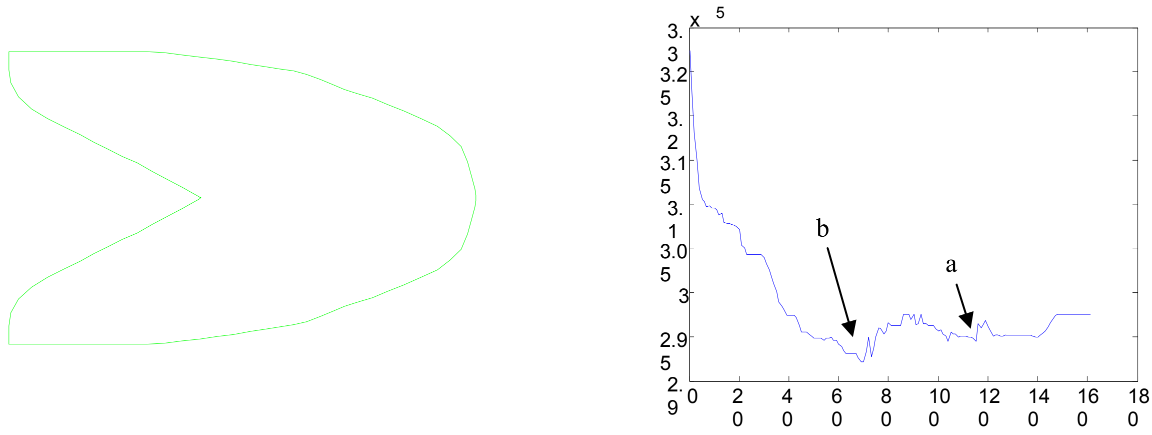

(a) Optimal short cantilever beam

(b) S-history of CV

Figure 9: Results for short cantilever beam

There are various other S-history local minima; some are produced by the convergence of oscillations which increase the control point direction parameter d_i and others are from the convergence of solutions. The S-history single-run-global minimum occurs at iteration 70, labelled ‘b’ on Figure 9(b) and has a volume reduction of 17% and is shown in Figure 10. The S-history single-rum-global minimum has a similar shape to the local solution of Figure 9(a) in that the material has been removed from the corners on the right hand side and in a triangular shape void has formed on the left hand side. The larger minimum of Figure 10 is favoured over Figure 9(a) as the strain energy within the structure increases as the volume decreases and there will be a concentration of strain energy increasing at the tip of the triangular shape formed on the left hand side. This strain energy concentration, which increases as the volume decreases, increases S(x) by less than 1%.

If topology optimisation were to be performed, the holes that would be created within the structure would stop the triangular shape moving too far into the structure and would thus limit the strain energy concentration at the tip.

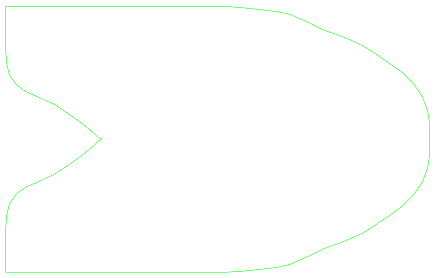

Figure 10: S-history single-rum global minimum

8. Topology optimisation

8.1. Topology optimisation algorithm

To implement topology optimisation, the algorithm detailed in section 6.3 needs the following modification after step 8:

1. Search for elements with the lowest sensitivity S_e.
2. If the elements with the minimum value for S_e satisfy $S_e < \mathrm{d_i}$ the then create a hole at the locations of those elements. Holes are created by inserting a closed spline with 4 points around the element where the hole is created. The 4 control points are place in the centres of the 4 elements that are on the diagonal of the removed element as in …

3. In a similar manner to step 8, the distances between the new spline and the existing splines require calculation. However, this time, if each control point satisfies (15), as in fig… for the user defined parameter ζ, the two boundaries are to be merged. Two boundaries are merged by removing the control points that are too close to one another and the remaining control points form the new boundary as in fig…

$$\| \mathbf{c}_j - \mathbf{c}_k \|_2 < \zeta . \qquad (15)$$

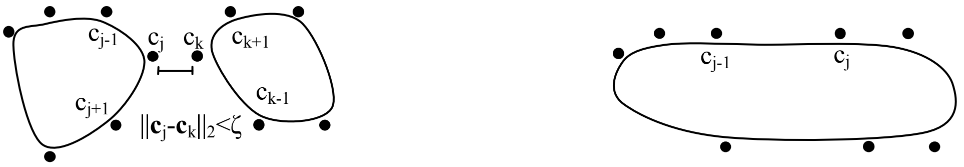

(a) Two control points that satisfy (15)

(b) Hole merged into one

Figure 11: Merging holes

4. Determine the new distances between control points for the merged holes as in steps 0 and 8.b of the shape optimisation algorithm
5. Continue with step 9 of shape optimisation algorithm.

8.2. Preliminary results

Boundary based topology optimisation using FG is preliminarily applied to a simplified short cantilever whereby the applied load is moved to the bottom right hand corner of the structure rather than midway through the right hand side. Fig… shows iteration ??? whereby 3 now holes are introduced in the centre of the structure at (a) from ?? and within the same iteration, the holes are merges as detailed in ??? leaving one larger hole as in (b).

After 49 iterations, di has converged to 0.21 and several holes have been introduced as in fig???(a). fig???(b) then has the shistory to that point, which is also the s-history single run global at iteration 49 The volume reduction is …

Further iterations see the holes merging with the outer boundary, which is not something you would expect. Further development on when holes are merge is required

9. Conclusions

Structural optimisation has been implemented using an efficient linear solver, within a Fixed Grid environment which uses B-splines to represent a structures boundary and has a mathematically based optimality conditions.

The linear solver used was a direct method known as a multifrontal solver. This multifrontal solver was chosen after a series of investigations showed that it was the fastest direct solver for the class of problems created by the FG environment. The investigations also revealed that the multifrontal solver is faster than the iterative conjugate gradient solver using a Jacobi pre-conditioner.

Using B-splines to represent the boundaries of a structure have successfully produced smooth topologies.

In addition, the optimisation algorithm for existing boundaries are extended to create holes and merge holes, and a preliminary result for this effort is presented. The result suggest that

10. Acknowledgements

The authors thank Prof Iain Duff, Rutherford Appleton Laboratory for his useful advise and discussion on linear solvers and Dr Lars Krog, Airbus UK for his inspiring and helpful comments and suggestions. The authors would also like to thank Numerical Analysis group at the Rutherford Appleton Lab for their FORTRAN HSL packages. The authors acknowledge the support of UK Engineering and Physical Sciences Research Council (GR\ S68477) for this research.

11. References

1. Zhou M, Rozvany GIN. On the validity of ESO type methods in topology optimization. Struct Multidisc Optim, 2001, 21: 80-83
2. Edwards CS, Kim HA, Budd CJ. An evaluative study on ESO and SIMP for optimising a cantilever tie-beam. Struct Multidisc Optim, 2007, Online first
3. Bendsøe MP. Optimal shape design as a material distribution problem. Springer, Berlin, 1989
4. Rozvany GIN, Zhou M, Birker T. Generalized shape optimisation without homogenisation, Struct Optim, 1992, 4:250-254
5. Bendsøe MP, Sigmund O. Topology optimization: theory, methods and applications. Springer, Berlin, 2003
6. Stolpe M, Svanberg K. On the trajectories of penalization methods for topology optimization. Struct Multidisc Optim, 2001, 21:128-139

7. Kim H, Querin OM, Steven GP, Xie YM. A method for varying the number of cavities in an optimized topology using evolutionary structural optimization. Struct Multidisc Optim, 2000, 19:140-147
8. Jog CS, Haber RB. Stability of finite element models for distributed-parameter optimization and topology design. Comput Methods Appl Mech Eng, 1996, 130:203-226
9. Díaz A, Sigmund O. Checkerboard patterns in layout optimization. Struct Optim, 1995, 10:40-45
10. Sigmund O, Petersson J. Numerical instabilities in topology optimization: a survey on procedures dealing with checkerboards, mesh-dependencies and local minima. Struct Optim, 1998, 16:68-75
11. García MJ. Fixed grid finite element analysis in structural design and optimisation. PhD thesis, University of Sydney, Australia, 1999
12. Kim H, Garcia MJ, Querin OM, Steven GP. Introduction of fixed grid in evolutionary structural optimisation. Engineering Computations, 2000, 17(4):427-439
13. Moës N, Dolbow J, Belytschko T. A finite element method for crack growth without remeshing. Int J Numer Meth Engrg, 1999,46:131-150
14. Sethian JA. Level set methods and fast marching methods: evolving interfaces in computational geometry, fluid mechanics, computer vision, and materials science. Cambridge University Press, Cambridge, UK, 1999
15. Wang M, Wang X, Guo D. A level set method for structural topology optimization. Comput Methods Appl Mesh Engrg, 2003, 192:227-246
16. Allaire G, Jouve F, Toader AM. Structural Optimization using sensitivity analysis and a level-set method. J Comp Phys, 2004, 194:363-393
17. Sokolowski J, Żochowski A. On the topological derivative in shape optimization. SIAM J Control Optim, 1999, 37(4):1251-1272
18. Burger M, Hackl B, Ring W. Incorporating derivatives into level set methods. J Comp Phys, 2004, 194:344-362
19. Allaire G, de Gournay F, Jouve F, Toader AM. Structural optimization using topological and shape sensitivity via a level set method. Control and Cybernetics, 2005, 34(1):59-80
20. Norato JA, Bendsøe MP, Haber RB, Tortorelli DA. A topological derivative method for topology optimization. Struct Multidisc Optim, 2007, 33:375-386
21. Michell AGM. The limits of economy of material in frame-structures. Philos Mag, 1904, 8:589-597
22. Duff IS, Erisman AM, Reid JK. Direct methods for sparse matrices. Oxford University Press, Oxford, UK, 1986
23. Rutherford Appleton Laboratory. Harwell subroutine library. Numerical Analysis Group, Chilton, Oxfordshire, UK, 2004
24. Trevelyan J, Scales DJ, Morris R, Bird GE. Acceleration of boundary element computations in reanalysis of problems in elasticity. WCCM VI in conjunction with APCOM'04, Beijing, China, 2004
25. Golub GH, Van Loan CF. Matrix computations 3rd ed. Johns Hopkins University Press, Baltimore, USA,1996
26. Garcia MJ, Gonzalez CA. Shape optimisation of continuum structures via evolution strategies and fixed grid finite element analysis. Struct Multidisc Optim, 2004, 26:92-98
27. Bobaru F, Rachakonda S. E(FG)2: a new fixed grid shape optimization method based on the element-free galerkin mesh-free analysis. Struct Multidisc Optim, 2006, 32:215-228
28. Tanskanen P. The evolutionary structural optimization method: theoretical aspects. Comput Methods Appl Mech Eng, 2002, 191:5485-5498
29. Komzsik L. Approximation techniques for engineers. CRC Press, Taylor and Francis Group, Boca Raton, 2007
30. The Math Works. Matlab 7.0. The Math Works, Matick, MA, USA, 2004